THEF-NIJM 23.01

Quark phases in neutron stars consistent with implications of NICER

Y. Yamamoto[1],* N. Yasutake[2], and Th.A. Rijken[31]

[1]*RIKEN Nishina Center, 2-1 Hirosawa, Wako, Saitama 351-0198, Japan*
[2]*Department of Physics, Chiba Institute of Technology,*
2-1-1 Shibazono Narashino, Chiba 275-0023, Japan
[3]*IMAPP, Radboud University, Nijmegen, The Netherlands*

Abstract

The analyses for the NICER data imply $R_{2.0M_\odot} = 12.41^{+1.00}_{-1.10}$ km and $R_{1.4M_\odot} = 12.56^{+1.00}_{-1.07}$ km, indicating the lack of significant variation of the radii from $1.4M_\odot$ to $2.0M_\odot$. This feature cannot be reproduced by the hadronic matter due to the softening of equation of state (EoS) by hyperon mixing, indicating the possible existence of quark phases in neutron-star interiors. Two models are used for quark phases: In the quark-hadron transition (QHT) model, quark deconfinement phase transitions from a hadronic-matter EoS are taken into account so as to give reasonable mass-radius (MR) curves by adjusting the quark-quark repulsions and the density dependence of effective quark mass. In the quarkyonic model, the degrees of freedom inside the Fermi sea are treated as quarks and neutrons exist at the surface of the Fermi sea, where MR curves are controlled mainly by the thickness of neutron Fermi layer. The QHT and quarkyonic EoSs can be adjusted so as to reproduce radii, tidal deformabilities, pressure and central densities inferred from the NICER analysis better than the nucleonic matter EoS, demonstrating the clear impacts of quark phases. Then, the maximum mass for the quakyonic-matter EoS is considerably larger than that for the QHT-matter EoS.

PACS numbers: 21.30.Cb, 21.30.Fe, 21.65.+f, 21.80.+a, 12.39.Jh, 25.75.Nq, 26.60.+c

*Electronic address: yamamoto@tsuru.ac.jp

I. INTRODUCTION

In studies of neutron stars (NS), the fundamental role is played by the equation of state (EoS) for neutron star matter. The massive neutron stars with masses over $2M_\odot$ have been reliably established by the observations of NSs J1614−2230 [1], J0348+0432 [2], J0740+6620 [3] and J0952-0607 [4]. The radius information of NSs have been obtained for the massive NS PSR J0740+6620 with $2M_\odot$ and $1.4M_\odot$ NSs, shown as $R_{2M_\odot}$ and $R_{1.4M_\odot}$, from the analyses for the X-ray data taken by the *Neutron Star Interior Composition Explorer* (NICER) and the X-ray Multi-Mirror (XMM-Newton) observatory. The analysis of Miller et al. gives $R_{2.08M_\odot} = 12.35 \pm 0.75$ km and $R_{1.4M_\odot} = 12.45 \pm 0.65$ km [5]. The analysis of Riley gives $R_{2.08M_\odot} = 12.39^{+1.30}_{-0.98}$ km and $R_{1.4M_\odot} = 12.33^{+0.76}_{-0.81}$ km [6]. Legred et al. investigate these measurement's implications for the EoSs, employing a nonparametric EoS model based on Gaussian processes and combining information from other X-ray and gravitational wave observations [7].

The purpose of this paper is to demonstrate that the radius information of massive NSs give the important constraints for the neutron-star EoSs. In our EoS analysis, the following neutron-star radii are adopted as critical values to be reproduced:

$$\begin{aligned} R_{2.0M_\odot} &= 12.41^{+1.00}_{-1.10} \text{ km} \\ R_{1.4M_\odot} &= 12.56^{+1.00}_{-1.07} \text{ km} \end{aligned} \tag{1.1}$$

with maximum mass $M_{max}/M_\odot = 2.21^{+0.31}_{-0.21}$, being given by the analysis by Legred et al.[7]. The median values of $R_{2M_\odot}$ and $R_{1.4M_\odot}$ in the above three references [5][6][7] are only a few hundred meters apart from each other. We set the fitting accuracy to a few hundred meters in our analysis for $R_{2M_\odot}$ and $R_{1.4M_\odot}$. Then, the EoS obtained from our analysis are not changed, even if the set of $R_{2M_\odot}$ and $R_{1.4M_\odot}$ in [5] or [6] is used as the criterion instead of Eq.(1.1) or all three sets in [5][6][7] are used. The key feature found commonly in the three sets is the small variation of radii from $1.4M_\odot$ to $2M_\odot$, namely $R_{2M_\odot} \approx R_{1.4M_\odot}$. The reason why the result in [7] is used in our present analysis is because they present the inferred values of maximum masses, radii, tidal deformabilities, pressure and central densities obtained from their analysis. These quantities can be compared with our corresponding results, by which the features of our EoSs are revealed in detail.

The hyperon mixing in neutron-star matter brings about a remarkable softening of the EoS and a maximum mass is reduced to a value far less than $2M_\odot$. The EoS softening is caused by changing of high-momentum neutrons at Fermi surfaces to low-momentum hyperons via strangeness non-conserving weak interactions overcoming rest masses of hyperons. In order to derive EoSs for massive NSs, it is necessary to solve this "hyperon puzzle in neutron stars". There have been proposed possible mechanisms: (i) more repulsive hyperon-hyperon interactions in relativistic mean field (RMF) models driven by vector mesons exchanges [8–11], (ii) repulsive hyperonic three-body forces [12–19], (iii) appearance of other hadronic degrees of freedom, such as Δ isobars [20] or meson condensates [21–25], (iv) existence of quark phases in high-density regions [26–36]. It should be noted that the criterion for NS radii Eq.(1.1) is stricter than the condition of $M_{max} > 2M_\odot$ only to solve the "puzzle" and the above mechanisms are needed to be re-investigated under this stricter condition.

One of the approaches belonging to (ii) is to assume that three-nucleon repulsions (TNR) [37] work universally among every kind of baryons as three-baryon repulsions (TBR) [12]. In [14–16], the multi-pomeron exchange potential (MPP) was introduced as a model of universal repulsions among three and four baryons on the basis of the extended soft core (ESC) baryon-

baryon interaction model developed by two of the authors (T.R. and Y.Y.) and M.M. Nagels [39–41]. In the case of this special modeling for hyperonic three-body repulsions, the EoS softening by hyperon mixing is not completely recovered by the above universal repulsions, and the maximum masses become not so large even if universal many-body repulsions increase. As a result, the maximum masses for hyperonic-matter EoS cannot be over $2M_{\odot}$, as found in [14–16]: It is difficult that criterion Eq.(1.1) is realized by this modeling of hadronic-matter EoSs. A simple way to avoid the strong softening of EoS by hyperon mixing is to assume ΛNN repulsions stronger than NNN repulsions with neglect of Σ^- mixing [17].

In this paper, we focus on the mechanism (iv). It is possible to solve the "hyperon puzzle" by taking account of quark deconfinement phase transitions from a hadronic-matter EoS to a sufficiently stiff quark-matter EoS in the neutron-star interiors, namely by studying hybrid stars having quark matter in their cores, where repulsive effects in quark phases are needed to result in massive stars over $2M_{\odot}$. In the Nambu-Jona-Lasinio (NJL) model, for instance, repulsions to stiffen EoSs are given by vector interactions. Then, it is known well that quark-hadron phase transitions should be crossover or at most weak first-order, because strong first-order transitions soften EoSs remarkably in order to obtain stiff EoSs. In [35], they derived the new EoS within the quark-hadron crossover (QHC) framework (3-windows model) so as to reproduce $R_{2.1M_{\odot}} \approx R_{1.4M_{\odot}} \approx$ 12.4km. Here, the small variation of radii indicates that the pressure grows rapidly while changes in energy density are modest, producing a peak in the speed of sound [35]. In their QHC framework, the EoSs in the quark-hadron mixed region of $1.5\rho_0 \sim 3.5\rho_0$, playing a decisive role for the resulting MR curves, are given by the interpolating functions phenomenologically. Then, it is meaningful to study the other modeling for phase transitions in which the mixed regions are modeled explicitly. We investigate how this criterion Eq.(1.1) can be realized in the case of using the EoS derived from our quark-hadron transition (QHT) model for neutron-star matter in the Bruecner-Hartree-Fock (BHF) framework [36], being different from their 3-windows model. Here, the quark-matter EoS is derived from the two-body quark-quark (QQ) potentials, in which all parameters are on the physical backgrounds with no room for arbitrarily changing: They are composed of meson-exchange quark-quark potentials derived by unfolding of the baryon-baryon meson-exchanges, and instanton-exchange, one-gluon-exchange and multi-pomeron exchange potentials. Then, baryonic matter and quark matter are treated in the common BHF framework, where quark-hadron transitions are treated on the basis of the Maxwell condition. In this paper, it is shown that the criterion Eq.(1.1) can be realized by our QHT model for neutron-star matter, as well as the QHC model [35], by adjusting the QQ repulsion to be strong enough and the quark-hadron transition density to be about $2\rho_0$.

In our QHT model the BHF framework is used for deriving the quark-matter EoS, which is not popular. Our treatments for quark-hadron phase transitions is the same as that in [33] where the NJL model is adopted for quark matter under the mean field approximation. In spite of the difference between quark-matter models, their obtained MR curves are similar to ours in [36]. Therefore, it is considered that the same conclusions can be derived also by using their QHT model instead of ours.

Another type of quark phase in neutron-star interiors is given by the quarkyonic matter [43–50], where the degrees of freedom inside the Fermi sea are treated as quarks and nucleons exist at the surface of the Fermi sea. The transition from hadronic-matter phase to the quarkyonic-matter phase is considered to be in second-order. In the quarkyonic matter, the existence of free quarks inside the Fermi sea gives nucleons extra kinetic energy by pushing them to higher momenta, leading to increasing pressure. This mechanism to realize the criterion Eq.(1.1) is completely different from the QHT matter in which the essential roles for EoS stiffening are played by the QQ repulsions. Then, it is valuable to study the characteristic differences between neutron-star mass-radius (MR) curves obtained from the QHT-matter EoS and quarkyonic-matter EoS.

This paper is organized as follows: In Sect.II, the hadronic-matter EoS (II-A), the quark-matter EoS (II-B) and the quarkyonic-matter EoS (II-C) are formulated on the basis of our previous works, where the BHF frameworks with our QQ potentials are adopted both for baryonic matter and quark (quarkyonic) matter. Transitions from hadron phases to quark matter (quakyonic) phases are explained. In Sect.III-A, the calculated results are shown for pressures, energy densities and sound velocities. In III-B, the MR curves of hybrid stars are obtained by solving the Tolmann-Oppenheimer-Volkoff (TOV) equation. In III-C, the obtained values of maximum masses, radii, tidal deformabilities, pressure and central densities are compared with those inferred from the NICER-data analysis. The conclusion of this paper is given in Sect.IV.

II. MODELS OF NEUTRON-STAR MATTER

A. hadronic matter

The hadronic matter is defined as β-stable hyperonic nuclear matter including leptons, composed of n, p^+, Λ, Σ^-, e^-, μ^-. We recapitulate here the hadronic-matter EoS. In the BHF framework, the EoS is derived with use of the ESC baryon-baryon (BB) interaction model [14–16].

As is well known, the nuclear-matter EoS is stiff enough to assure neutron-star masses over $2M_\odot$, if the strong three-nucleon repulsion (TNR) is taken into account. However, there appears a remarkable softening of EoS by inclusion of exotic degrees of freedom such as hyperon mixing. One of the ideas to avoid this "hyperon puzzle" is to assume that the many-body repulsions work universally for every kind of baryons [12]. In [14–16], the multi-pomeron exchange potential MPP was introduced as a model of universal repulsions among three and four baryons. This was inspired by the multi-reggeon model to describe CERN-ISR pp-data [38]. The ESC work is mentioned in [39–41].

In [16] they proposed three versions of MPP (MPa, MPa$^+$, MPb), where MPa and MPa$^+$ (MPb) include the three- and four-body (only three-body) repulsions. Their strengths are determined by analyzing the nucleus-nucleus scattering using the G-matrix folding model under the conditions that the saturation parameters are reproduced reasonably. The EoSs for MPa and MPa$^+$ are stiffer than that for MPb, and maximum masses and radii of neutron stars obtained from MPa, MPa$^+$ are larger than those from MPb. The important criterion for repulsive parts is the resulting neutron-star radii R for masses of $1.4M_\odot$: In the case of using MPb, we obtain $R_{1.4M_\odot} \approx 12.4$ km similar to the value in the criterion Eq.(1.1). On the other hand, we have $R_{1.4M_\odot} \approx 13.3$ (13.6) km in the case of MPa (MPa$^+$). In this paper, we adopt MPb as three-baryon repulsion: Our nuclear interactions are composed of two-body part V_{BB} and three-body part V_{BBB}, where V_{BB} and V_{BBB} are given by ESC and MPb, respectively. It is worthwhile to say that the three-nucleon repulsion in MPb is stronger than the corresponding one (UIX) in the standard model by APR [37] giving rise to $R_{1.4M_\odot} \approx 11.6$ km [42].

BB G-matrix interactions $\mathcal{G}_{BB}$ are derived from BB bare interactions V_{BB} or $V_{BB}+V_{BBB}$ [14]. They are given for each (BB', T, S, P) state, T, S and P being isospin, spin and parity in a two-body state, respectively, and represented as $\mathcal{G}^{TSP}_{BB'}$. The G-matrix interactions derived from V_{BB}

and $V_{BB}+V_{BBB}$ are called B1 and B2, respectively. In the quarkyonic model, we need only the neutron-neutron sectors, $\mathcal{G}^{SP}_{nn}$.

A single baryon potential is given by

$$\begin{aligned} U_B(k) &= \sum_{B'=n,p,\Lambda,\Sigma^-} U_B^{(B')}(k) \\ &= \sum_{B'=n,p,\Lambda,\Sigma^-} \sum_{k'<k_F^{(B')}} \langle kk'|\mathcal{G}_{BB'}|kk'\rangle \end{aligned} \tag{2.1}$$

with $B = n, p, \Lambda, \Sigma^-$. Here, $\langle kk'|\mathcal{G}_{BB'}|kk'\rangle$ is a BB' G-matrix element in momentum space, being derived from V_{BB} or $(V_{BB}+V_{BBB})$, and $k_F^{(B)}$ is the Fermi momentum of baryon B. In this expression, spin and isospin quantum numbers are implicit.

The baryon energy density is given by

$$\begin{aligned} \varepsilon_B &= \tau_B + \upsilon_B \\ &= g_s \int_0^{k_F^{(B)}} \frac{d^3k}{(2\pi)^3} \left\{ \sqrt{\hbar^2 k^2 + M_B^2} + \frac{1}{2} U_B(k) \right\} , \end{aligned} \tag{2.2}$$

where τ_B and υ_B are kinetic and potential parts of the energy density.

In β-stable hadronic matter composed of n, p, e^-, μ^-, Λ and Σ^-, equilibrium conditions are given as

(1) chemical equilibrium conditions,

$$\mu_n = \mu_p + \mu_e \tag{2.3}$$
$$\mu_\mu = \mu_e \tag{2.4}$$
$$\mu_\Lambda = \mu_n \tag{2.5}$$
$$\mu_{\Sigma^-} = \mu_n + \mu_e \tag{2.6}$$

(2) charge neutrality,

$$\rho_p = \rho_e + \rho_\mu + \rho_{\Sigma^-} \tag{2.7}$$

(3) baryon number conservation,

$$\rho = \rho_n + \rho_p + \rho_\Lambda + \rho_{\Sigma^-} \ . \tag{2.8}$$

Expressions for β-stable nucleonic matter composed of n, p, e^- and μ^- are obtained by omitting hyperon sectors from the above expressions for β-stable baryonic matter.

B. Quark-Hadron transition model

In our treatment of quark matter, the BHF framework is adopted on the basis of two-body QQ potentials [36]. Here, correlations induced by bare QQ potentials are renormalized into coordinate-space G-matrix interactions, being considered as effective QQ interactions used in quark-matter calculations.

Our bare QQ interaction is given by

$$V_{QQ} \;=\; V_{EME} + V_{INS} + V_{OGE} + V_{MPP} \tag{2.9}$$

where V_{EME}, V_{INS}, V_{OGE} and V_{MPP} are the extended meson-exchange potential, the instanton-exchange potential, the one-gluon exchange potential and the multi-pomeron exchange potential, respectively. Parameters in our QQ potential are chosen so as to be consistent with physical observables. The V_{EME} QQ potential is derived from the ESC BB potential so that the QQM couplings are related to the BBM couplings through folding procedures with Gaussian baryonic quark wave functions. In the construction of the relation between BBM and QQM couplings, the requirement that the coefficients of the $1/M^2$ expansion should match is based on Lorentz invariance, which fixes the QQM couplings and also determines the (few) extra vertices at the quark level [39]. Then, the V_{EME} QQ potential is basically of the same functional expression as the ESC BB potential. Strongly repulsive components in ESC BB potentials are described mainly by vector-meson and pomeron exchanges between baryons. This feature persists in the V_{EME} QQ potential, which includes the strongly repulsive components originated from vector-meson and pomeron exchanges between quarks. Similarly the multi-pomeron exchange potentials among quarks, V_{MPP}, are derived from the corresponding ones among baryons, giving repulsive contributions. Contributions from V_{INS} and V_{OGE} in average are attractive and repulsive, respectively. The strength of V_{OGE} is determined by the quark-gluon coupling constant α_S. In [36] α_S is chosen as 0.25, that is $V_{OGE}(\alpha_S = 0.25)$, and the three sets are defined as follows: Q0 : V_{EME}, Q1 : $V_{EME} + V_{INS} + V_{OGE}(\alpha_S = 0.25)$ Q2 : $V_{EME} + V_{MPP} + V_{INS} + V_{OGE}(\alpha_S = 0.25)$.

In our QHT model for neutron-star matter, quark-hadron phase transitions occur at crossing points of hadron pressure $P_H(\mu)$ and quark pressure $P_Q(\mu)$ being a function of chemical potential μ. Positions of crossing points, giving quark-hadron transition densities, are controlled by parameters ρ_c and γ included in our density-dependent quark mass

$$M_Q^*(\rho_Q) = \frac{M_0}{1+\exp[\gamma(\rho_Q-\rho_c)]} + m_0 + C \tag{2.10}$$

with $C = M_0 - M_0/[1+\exp(-\gamma\rho_c)]$ assuring $M_Q^*(0) = M_0 + m_0$, where ρ_Q is number density of quark matter, and M_0 and m_0 are taken as 300 (360) MeV and 5 (140) MeV for u and d (s) quarks. Here, the effective quark mass $M_Q^*(\rho_Q)$ should be used together with $B(\rho_Q) = M_Q^*(0) - M_Q^*(\rho_Q) + B_0$, meaning the energy-density difference between the perturbative vacuum and the true vacuum. A constant term B_0 is added for fine tuning of an onset density. In [36], the values of (ρ_c, γ) without B_0 are given for each set of Q0, Q1 and Q2.

Let us focus on the typical result for Q2+H1 in [36]. The QQ interaction Q2 is the most repulsive among Q0, Q1 and Q2. The BB interaction H1 consists of ESC and MPb, and results in the reasonable value of $R_{1.4M_\odot}$. In this case of Q2+H1, we obtain the maximum mass of $2.25M_\odot$ and the reasonable value of $R_{1.4M_\odot} = 12.5$ km, in which the quark-hadron transition occurs at density of $3.5\rho_0$. Then, we have $R_{2.0M_\odot} = 12.0$ km, being rather smaller than 12.4 km in the criterion Eq.(1.1). In order to reproduce a larger value of $R_{2.0M_\odot} \approx 12.4$ km, we make V_{OGE} more repulsive by taking larger values of $\alpha_S = 0.36$ and 0.49. It is not suitable for such a purpose to strengthen the V_{MPP} repulsion, because V_{MPP} is essentially of three-body interaction and the contributions in low-density region are small. On the other hand, V_{OGE}

is of two-body interaction, and its repulsive contributions are not small even in low density region, being important for a large value of $R_{2.0M_\odot}$. Another condition to make $R_{2.0M_\odot}$ larger is to lower quark-hadron transition densities by adjusting the parameters (ρ_c,γ,B_0) included in the density-dependent quark mass Eq.(2.10).

We define newly the following three sets with the fixed value of γ=1.2

Q2 : $V_{EME} + V_{MPP} + V_{INS} + V_{OGE}(\alpha_S = 0.25)$
with $\rho_c = 6.9\rho_0$ and B_0 =8.5
Q3 : $V_{EME} + V_{MPP} + V_{INS} + V_{OGE}(\alpha_S = 0.36)$
with $\rho_c = 6.9\rho_0$ and B_0 =7.5
Q4 : $V_{EME} + V_{MPP} + V_{INS} + V_{OGE}(\alpha_S = 0.69)$
with $\rho_c = 7.5\rho_0$ and B_0 =10.0

where the values of ρ_c and B_0 for each set are chosen so as to give quark-hadron transition densities of $\sim 2\rho_0$.

G-matrix interactions $\mathcal{G}_{qq'}$ with $q, q' = u, d, s$ are derived from the above bare QQ interactions. They are given for each (qq', T, S, P) state, T, S and P being isospin, spin and parity in a two-body state, respectively, and represented as $\mathcal{G}^{TSP}_{qq'}$. Hereafter, Q2, Q3 and Q4 mean the naming of corresponding QQ G-matrix interactions, not only of bare QQ interactions. The QQ G-matrix interactions are used also in the quarkyonic matter calculations.

A single quark potential is given by

$$U_q(k) = \sum_{q'=u,d,s} U_q^{(q')}(k) = \sum_{q'=u,d,s} \sum_{k'<k_F^{q'}} \langle kk'|\mathcal{G}_{qq'}|kk'\rangle \tag{2.11}$$

with $q = u, d, s$, where k_F^q is the Fermi momentum of quark q. Spin and isospin quantum numbers are implicit.

The quark energy density is given by

$$\varepsilon_q = g_s N_c \sum_{q=u,d,s} \int_0^{k_{Fq}} \frac{d^3k}{(2\pi)^3} \left\{\sqrt{\hbar^2k^2 + M_q^2} + \frac{1}{2}U_q(k)\right\} . \tag{2.12}$$

Fermion spin and quark color degeneracies give rise to $g_s = 2$ and $N_c = 3$.

In order to demonstrate the features of our QQ interactions (Q2,Q3,Q4), we show the potential energy per particle U/A as a function of the baryon number density $\rho_B = \frac{1}{3}\rho_Q$ in the case of taking $\rho_u = \rho_d = \rho_s$. In Fig.1, the short-dashed, long-dashed and solid curves are obtained by using Q2, Q3 and Q4, respectively. The repulsions are found to be strong in the order of Q4, Q3, Q2. This difference of repulsions among Q4, Q3 and Q2 comes from the different values of α_S included in V_{OGE}. In the figure, it should be noted that the difference is not small even in the low-density region.

In the EoS of β-stable quark matter composed of u, d, s, e^-, the equilibrium conditions are given as

(1) chemical equilibrium conditions,

$$\mu_d = \mu_s = \mu_u + \mu_e \tag{2.13}$$

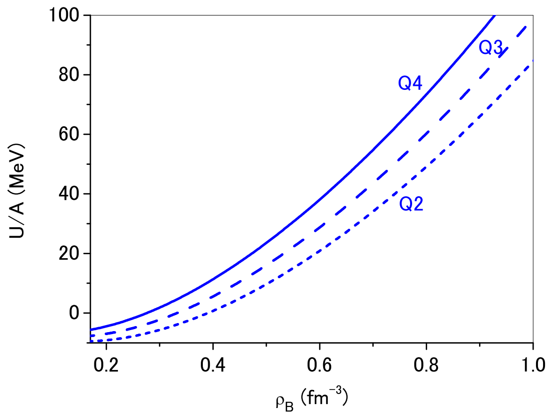

FIG. 1: (Color online) Potential energies per particle U/A as a function of the baryon number density ρ_B in the case of $\rho_u = \rho_d = \rho_s$. The short-dashed, long-dashed and solid curves are obtained by using Q2, Q3 and Q4, respectively.

(2) charge neutrality,

$$0 = \frac{1}{3}(2\rho_u - \rho_d - \rho_s) - \rho_e \tag{2.14}$$

(3) baryon number conservation,

$$\rho_B = \frac{1}{3}(\rho_u + \rho_d + \rho_s) = \frac{1}{3}\rho_Q\,. \tag{2.15}$$

In order to construct the hybrid EoS including a transition from hadronic phase to quark phase, we use the replacement interpolation method [33] [36], being a simple modification of the Maxwell and the Glendenning (Gibbs) constructions [51]. The EoSs of hadronic and quark phases and that of mixed phase are described with the relations between pressures and chemical potentials $P_H(\mu)$, $P_Q(\mu)$ and $P_M(\mu)$, respectively. The critical chemical potential μ_c for the transition from the hadronic phase to the quark phase is obtained from the Maxwell condition

$$P_Q(\mu_c) = P_H(\mu_c) = P_c\,. \tag{2.16}$$

The pressure of the mixed phase is represented by a polynomial ansatz. The matching densities ρ_H and ρ_Q are obtained with use of $\rho(\mu) = dP(\mu)/d\mu$.

C. quarkyonic matter

In the BHF framework, we derive the EoS of quarkyonic matter composed of neutrons and quarks with flavor $q = u, d$ in the simplest form by McLerran and Reddy [45]. In the chargeless 2-flavor quarkyonic matter, strongly interacting quarks near the Fermi sea form interacting neutrons, and the remaining d and u quarks fill the lowest momenta up to k_{Fu} and k_{Fd}, respectively. The quark mass is taken to be $M_q = M_n/3$ constantly, M_n being the neutron mass. In calculations of quarkyonic matter, we use B1 (V_{nn}) and B2 (V_{nn}+V_{nnn}) for nuclear interactions, and Q0 for QQ interactions for simplicity.

The total baryon number density is given by

$$\begin{aligned}\rho_B &= \rho_n + \frac{N_c}{3}(\rho_u + \rho_d) \\ &= \frac{g_s}{6\pi^2}\left[k_{Fn}^3 - k_{0n}^3 + \frac{N_c}{3}(k_{Fu}^3 + k_{Fd}^3)\right] , \end{aligned} \tag{2.17}$$

where k_{Fn}, k_{Fu} and k_{Fd} are the Fermi momenta of neutrons and u and d quarks, respectively. Fermion spin and quark color degeneracies give rise to $g_s = 2$ and $N_c = 3$. Neutrons are restricted near the Fermi surface by k_{0n}, being assumed as

$$\begin{aligned}k_{0n} &= k_{Fn} - \Delta_{qyc} \\ \Delta_{qyc} &= \frac{\Lambda^3}{\hbar c^3 k_{Fn}^2} + \kappa\frac{\Lambda}{N_c^2 \hbar c} , \end{aligned} \tag{2.18}$$

where Δ_{qyc} for the thickness of Fermi layer includes the two parameters Λ and κ. In this work, we take the fixed value of $\kappa = 0.3$.

Then, k_{Fd} and k_{Fu} are related to k_{0n} by $k_{Fd} = \frac{1}{N_c}k_{0n}$ and $k_{Fu} = 2^{-1/3}k_{Fd}$.

A single neutron potential is given by

$$U_n(k) = \sum_{k_{0n}<k'<k_{Fn}} \langle kk'|\mathcal{G}_{nn}|kk'\rangle \tag{2.19}$$

with nn G-matrix interactions $\mathcal{G}_{nn}$.

The neutron energy density is given by

$$\begin{aligned}\varepsilon_n &= \tau_n + \upsilon_n \\ &= g_s \int_{k_{0n}}^{k_{Fn}} \frac{d^3k}{(2\pi)^3}\left\{\sqrt{\hbar^2 k^2 + M_n^2} + \frac{1}{2}U_n(k)\right\} . \end{aligned} \tag{2.20}$$

Additionally, another form of the neutron potential energy density is defined as

$$\bar{\upsilon}_n = g_s \int_0^{k_n} \frac{d^3k}{(2\pi)^3}\left\{\frac{1}{2}U_n(k)\right\} , \tag{2.21}$$

which is used in [45] instead of υ_n.

Single quark potentials for $q = u, d$ are given by

$$\begin{aligned}U_q(k) &= \sum_{q'=u,d} U_q^{(q')}(k) \\ &= \sum_{q'=u,d}\sum_{k'<k_{Fq}} \langle kk'|\mathcal{G}_{qq'}|kk'\rangle \end{aligned} \tag{2.22}$$

$$U_q^{(n)}(k) = \sum_{k_{0n}<k'<k_{Fn}} \langle kk'|\mathcal{G}_{qn}|kk'\rangle \tag{2.23}$$

with G-matrix interactions $\mathcal{G}_{qq'}$ and $\mathcal{G}_{qn}$. Here, $\mathcal{G}_{qn}$ is the quark-neutron (Qn) interactions: We assume the simple model in which the potentials $\mathcal{G}_{qq'}$ are folded into the potentials $\mathcal{G}_{qn}$ with Gaussian baryonic quark wave functions. In Eqs.(2.19)(2.22)(2.23) spin quantum numbers are implicit.

The quark energy density is given by

$$\begin{aligned} \varepsilon_q \;=\; & g_s N_c \sum_{q=u,d} \int_0^{k_{Fq}} \frac{d^3k}{(2\pi)^3} \\ & \left\{ \sqrt{\hbar^2 k^2 + M_q^2} + \frac{1}{2} U_q(k) + U_{qn}(k) \right\} , \end{aligned} \tag{2.24}$$

where values of k_{Fq} are determined by

$$N_c k_{Fq} = k_{0n} \ . \tag{2.25}$$

Thus, our total energy density is given by

$$\varepsilon = \varepsilon_n + \varepsilon_d + \varepsilon_u \ . \tag{2.26}$$

The chemical potential μ_i ($i = n, d, u$) and pressure P are expressed as

$$\mu_i = \frac{\partial \varepsilon_i}{\partial n_i} \ , \tag{2.27}$$

$$P = \sum_{i=n,d,u} \mu_i n_i - \varepsilon \ , \tag{2.28}$$

where $\frac{\partial \varepsilon_i}{\partial n_i} = \frac{\partial \varepsilon_i}{\partial n_B} \frac{\partial n_B}{\partial n_i}$.

In our model, the phase transition from β-stable nucleonic matter to the quarkyonic matter occurs in second-order, resulting in the hybrid EoS including hadronic and quarkyonic EoSs. Then, the transition densities are controlled mainly by the parameter Λ: In this work, we choose the three values of Λ=380, 350 and 320 MeV with the fixed value of $\kappa = 0.3$. The transition densities for these values are $0.28 \sim 0.38$ fm^{-3} ($0.28 \sim 0.36$ fm^{-3}) in the case of using B1 (B2) for nuclear interactions. Hereafter, when a value of Λ=380 MeV is used, for instance, it is denoted as Λ380.

III. RESULTS AND DISCUSSION

A. EoS

In Fig.2, pressures P are drawn as a function of baryonic number density ρ_B. The dot-dashed curve is for the β-stable nucleonic-matter EoS, and the dotted one is for the β-stable hadronic-matter EoS with hyperon mixing. The latter is substantially below the former, demonstrating the EoS softening by hyperon mixing. Thin (thick) solid curves in the upper side are pressures in the quarkyonic matter for Λ350 and Λ320 (Λ380) with use of B1 for nuclear interactions. At the crossing points with the dot-dashed curve in the low-density side,

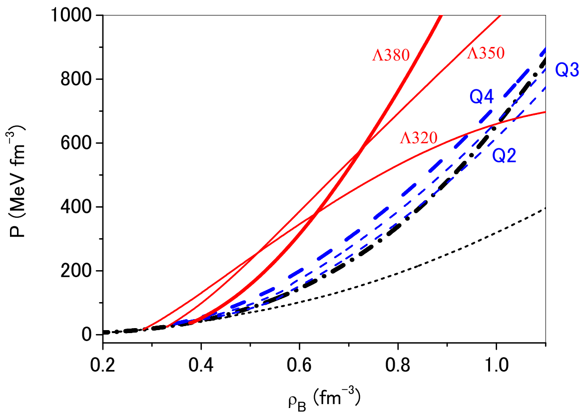

FIG. 2: (Color online) Pressures P as a function of baryonic number density ρ_B. The dot-dashed (dotted) curve is for β-stable nucleonic (hadronic) matter. Upper thin (thick) solid curves are pressures in the quarkyonic matter for Λ350 and Λ320 (Λ380) with B1. Lower thin (thick) short-dashed curves are for the QHT matter with Q2 and Q3 (Q4).

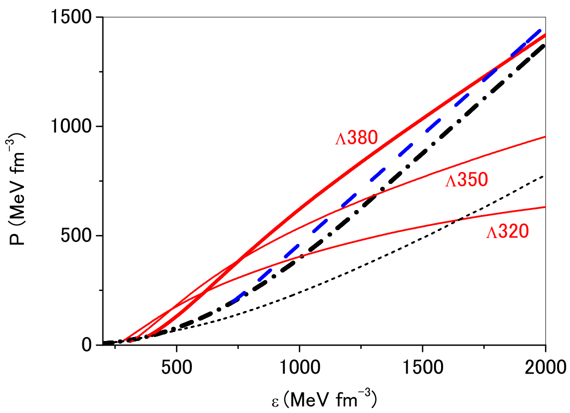

FIG. 3: (Color online) Pressures P as a function of the energy density ε. The dot-dashed (dotted) curves are for β-stable nucleonic (hadronic) matter. Thin (thick) solid curves show pressures in quarkyonic phases for Λ350 and Λ320 (Λ380) with B1. The short-dashed curve is for the QHT model with Q4.

there occur second-order transitions from β-stable nucleonic to quarkyonic phases: The transition densities ρ_t are 0.38, 0.33, 0.28 fm^{-3} ($2.2\rho_0$, $1.9\rho_0$, $1.6\rho_0$) in the cases of Λ380, Λ350 and Λ320, respectively. Thin (thick) short-dashed curves are for the QHT models with Q2 and Q3 (Q4). It should be noted that pressures in the quarkyonic matter increase more rapidly with density than those in the QHT matter. As discussed later, the rapid growth of pressure with density in the range of $2\rho_0 \sim 4\rho_0$ is an important feature of the quarkyonic model. This rapid increase of pressure at onset of the quarkyonic phase influences significantly on neutron-star MR curves.

In Fig.3, pressures P are drawn as a function of the energy density ε, which are related

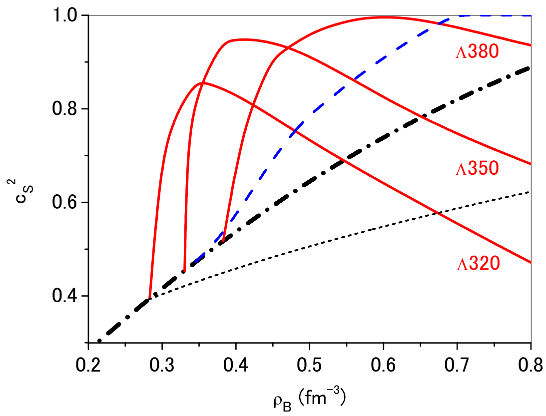

FIG. 4: (Color online) The square of the sound speed c_s^2 in units of c^2 as a function of baryonic number density ρ_B. The dot-dashed (dotted) curve is that in β-stable nucleonic (hadronic) matter. Solid curves are pressures in quarkyonic matter for Λ380, Λ350 and Λ320 with B1. The dashed curve is for the QHT matter with Q4.

closely to neutron-star *MR* curves. The dot-dashed (dotted) curve shows pressures in β-stable nucleonic (hadronic) matter. Thin (thick) solid curves show pressures in quarkyonic matter for Λ350 and Λ320 (Λ380) with B1. The short-dashed curve is for the QHT matter with Q4. Though the curves for Q4 and Λ380 are rather similar to each other in comparison with the corresponding curves in Fig.2, the former is still less steep than the latter in the region of low energy density. As shown later, the EoSs for the QHT model Q4 and the quarkyonic model Λ380 lead to the neutron-star *MR* curves consistent with the criterion Eq.(1.1).

In Fig.4, sound velocities are drawn as a function of ρ_B. The dot-dashed curve is sound velocities in β-stable nucleonic matter. Solid curves are those in quarkyonic matter for Λ380, Λ350 and Λ320 with B1. There appear peak structures in the solid curves, being related to rapid increasing of pressures in the range of $2\rho_0 \sim 4\rho_0$. The dashed curve is sound velocities in the QHT matter with Q4 and the dotted one is those in β-stable hadronic matter with hyperon mixing, in which there appears no peak structure. The dashed curve becomes $c_s > c$ in high-density region. Also, the peak regions of solid curves become $c_s > c$, if B2 is used instead of B1 for nuclear parts. In such regions of $c_s > c$, sound velocities are approximated to be $c_s = c$.

It is interesting to notice that the peak structures in our quarkyonic-matter results are somewhat similar to those for the QHC-matter EoS (QHC21) found in [35]. Our QHT-matter EoS gives no peak structure in sound velocities, being different from both of them.

In the left panel of Fig.5, solid curves show pressures in quarkyonic matter for Λ380 in the cases of using B1 and B2 for nuclear interactions, and short-dashed (dashed) curves are partial pressures of neutrons (quarks) in respective cases. The dot-dashed curve is pressures in β-stable nucleonic matter. Pressures in quarkyonic matter are found to be completely dominated by neutron partial pressures. In order to reveal the reason why neutron pressures in quarkyonic matter are far higher than those in β-stable nucleonic matter, we show the neutron chemical potentials in the cases of using B1 and B2 for nuclear interactions: In the right panel of Fig.5, neutron chemical potentials μ_n are drawn as a function of ρ_B. Lower and upper solid curves give neutron chemical potentials in quarkyonic matter for Λ380 in the cases of using B1 and B2, respectively. The dot-dashed curve gives neutron chemical potential in β-

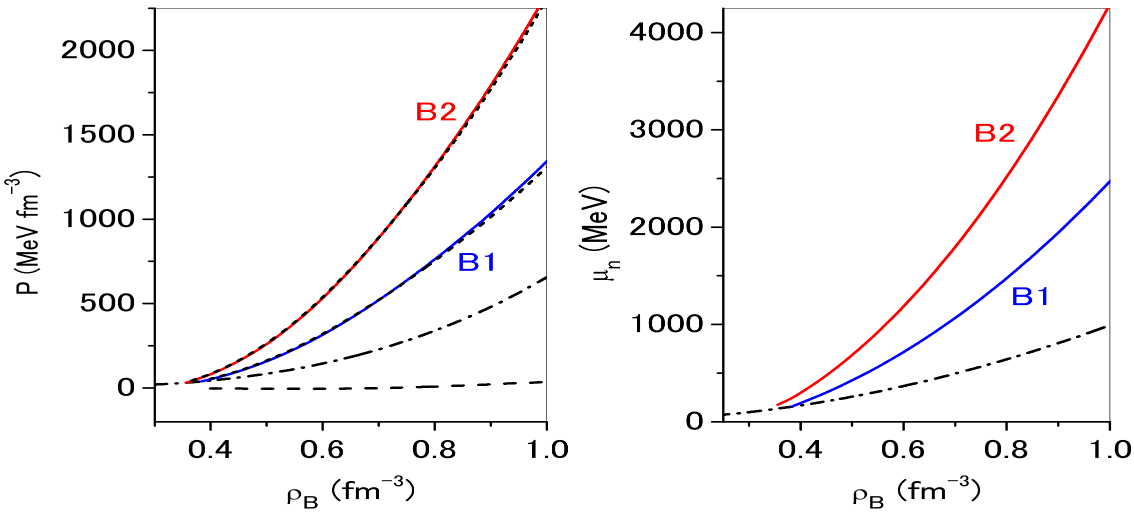

FIG. 5: (Color online) In the left panel, solid curves are pressures P in quarkyonic phases for as a function of baryonic number density ρ_B for $\Lambda380$ in the cases of using B1 and B2, and short-dashed (dashed) curves are partial pressures of neutrons (quarks) in respective cases. The dot-dashed curve is for β-stable nucleonic matter. In the right panel, solid (dot-dashed) curves are neutron chemical potentials μ_n in quarkyonic (β-stable nucleonic) phases as a function of ρ_B for $\Lambda380$ in the cases of using B1 and B2. The dot-dashed curve gives neutron chemical potential in β-stable nucleonic matter.

stable nucleonic matter. The neutron chemical potentials in quarkyonic matter are far higher than those in the β-stable nucleonic matter, which makes neutron pressures in the former far higher than those in the latter. The reason of higher chemical potentials in the quarkyonic matter is because the existence of free quarks inside the Fermi sea gives nucleons extra kinetic energies by pushing them to higher momenta [45].

B. *MR* diagrams

We have the two types of hybrid EoSs, the QHT-matter EoS and the quarkyonic-matter EoS. They are combined with the β-stable nucleonic-matter EoS connected smoothly to the crust EoS [52, 53] in the low-density side. The MR relations of hybrid stars can be obtained by solving the TOV equations with these hybrid EoSs.

In Fig.6, star masses are given as a function of radius R. The dot-dashed curves are obtained by the β-stable nucleonic matter EoS. In the left panel, thin (thick) solid curves are obtained by the QHT-matter EoSs with Q2 and Q3 (Q4). The dotted curve is by the hadronic-matter EoS including hyperons. In the cases of Q2, Q3 and Q4, the maximum masses are $M_{max}/M_\odot$= 2.23, 2.30, 2.40, respectively, and the radii at $2.0M_\odot$ are 11.8 km, 12.2 km, 12.5 km, respectively. In the right panel, thin (thick) solid curves are obtained by the quarkyonic-matter EoSs for $\Lambda350$ and $\Lambda320$ ($\Lambda380$) with use B1 for nuclear interactions. In the cases of $\Lambda380$, $\Lambda350$ and $\Lambda320$, the maximum masses are $M_{max}/M_\odot$= 2.64, 2.79, 2.76, respectively, and the radii at $2.0M_\odot$ are 12.6 km, 13.1 km, 13.5 km, respectively. In both panels, the horizontal lines indicates $R_{1.4M_\odot} = 12.56^{+1.00}_{-1.07}$ km and $R_{2.0M_\odot} = 12.41^{+1.00}_{-1.10}$ km, and the rectangle indicates the region of

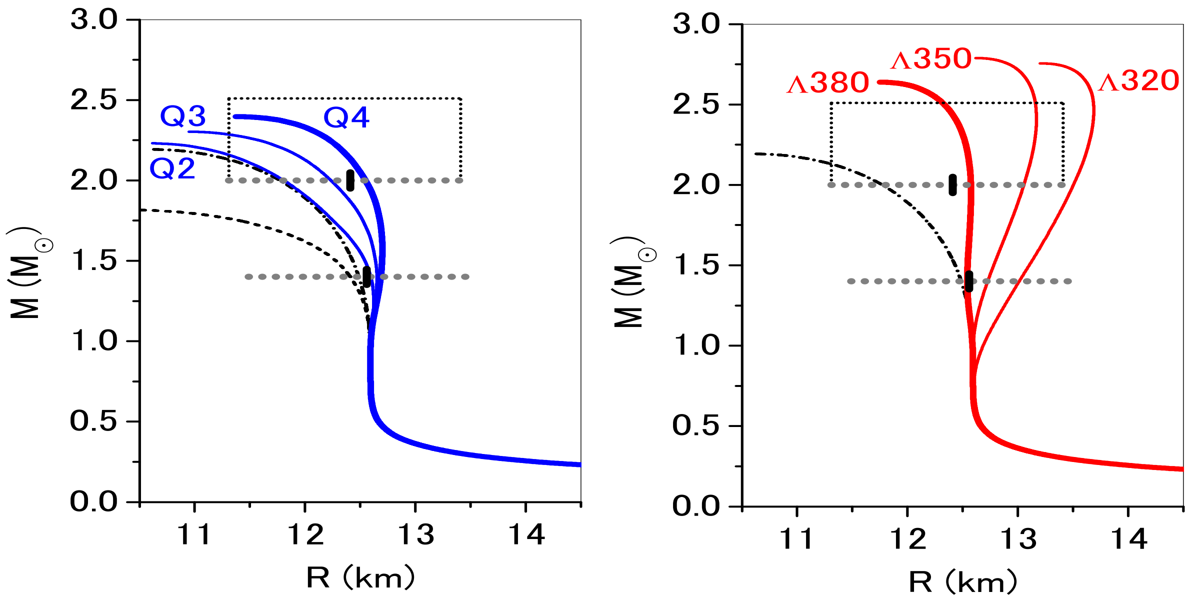

FIG. 6: (Color online) Star masses as a function of radius R. The dot-dashed curves are by the β-stable nucleonic matter EoS. In the left panel, thin (thick) solid curves are by the QHT-matter EoSs with Q2 and Q3 (Q4). The dotted curve is by the hadronic matter EoS including hyperons. In the right panel, thin (thick) solid curves are by the quarkyonic-matter EoSs for Λ350 and Λ320 (Λ380) with B1. In both panels, the horizontal lines indicates $R_{1.4M_\odot} = 12.56^{+1.00}_{-1.07}$ km and $R_{2.0M_\odot} = 12.41^{+1.00}_{-1.10}$ km, and the rectangle indicates the region of mass $M_{max}/M_\odot = 2.21^{+0.31}_{-0.21}$ [7].

mass $M_{max}/M_\odot = 2.21^{+0.31}_{-0.21}$ [7]. The thick solid curve for Q4 in the left panel and that for Λ380 in the right panel are found to be consistent with the criterion Eq.(1.1), and the key features of $R_{2M_\odot} \approx R_{1.4M_\odot}$ are found in these cases.

Then, it should be noted that the maximum mass $2.64M_\odot$ for Λ380 is substantially larger than the value $2.40M_\odot$ for Q4. The reason for such a difference between maximum masses can be understood by comparing the $P(\rho_B)$ curves in Fig.2, where the solid curve for Λ380 increases more rapidly at onset of the quakyonic matter than the dashed curve for Q4 at onset of quark matter. This means that the stiffness for former is larger than that for the latter. In the case of QHT matter, it is not possible to obtain such a rapid increasing of $P(\rho_B)$ in the low-density region, even if the QQ repulsions are strengthened.

In the case of hadronic (nucleonic) matter, shown by the dotted (dot-dashed) curve in the left panel, the maximum mass is $1.82M_\odot$ ($2.19M_\odot$). The reduction of $0.37M_\odot$ is due to the EoS softening by hyperon ((Λ and Σ^-) mixing. This softening is mainly caused by Σ^- mixing: If only Λ mixing is taken into account, the maximum mass is obtained as $2.06M_\odot$ being close to the value of $2.19M_\odot$ without hyperon mixing (dot-dashed curve). Thus, massive stars with $M > 2M_\odot$ cannot be obtained by the hadronic matter EoSs with hyperon (Λ and Σ^-) mixing [14–16]. On the other hand, the value of $R_{1.4M_\odot}$ is 12.4 (12.5) km in the case of hadronic (nucleonic) matter, which means that the hyperon mixing does not depend much on $R_{1.4M_\odot}$.

In Fig.7, star masses are given as a function of central baryon density ρ_{Bc}. The dot-dashed

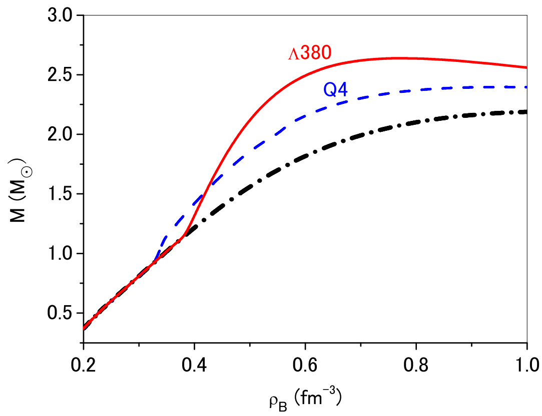

FIG. 7: (Color online) Star masses as a function of central baryon density ρ_{Bc}. The dot-dashed curves are by the β-stable nucleonic EoS. The solid curve is by the quarkyonic-matter EoS for Λ380 in the case of using B1. The short-dashed curve is by the QHT-matter EoS for Q4.

curves are by the β-stable nucleonic matter EoS. The solid curve is obtained by the quarkyonic-matter EoS for Λ380 with B1, and the dashed curve is by the QHT-matter EoS for Q4, where the onset density in the former (latter) 0.39 (0.33) fm^{-3}. Both of them are consistent with Eq.(1.1), but the former mass curve for ρ_{Bc} is considerably above the latter one, as well as the corresponding MR curves.

In Fig.8, star masses are given as a function of radius R. The solid curve is obtained by the quarkyonic-matter EoS for Λ380 with use of B1 (V_{nn}) for nuclear interactions, given also in Fig.6. Dashed and short-dashed curves are by the quarkyonic-matter EoSs for Λ380 and Λ400, respectively, in the case of using B2 (V_{nn}+V_{nnn}) instead of B1. The difference between solid and dashed curves demonstrates the effect of the three-neutron repulsion V_{nnn}, giving the larger maximum mass and larger value of $R_{2.0M_\odot}$. The short-dashed curve for Λ400 indicates that this effect of V_{nnn} to increase mass and radius is cancelled out by taking larger values of Λ.

In Fig.9, star masses are given as a function of radius R. The solid curve is obtained by the quarkyonic-matter EoS for Λ380 with $\kappa = 0.3$ in the case of using B1, given also in Fig.6. The dashed curve is obtained by the approximation used in [45], where the QQ interactions are neglected and the quark energy density Eq.(2.24) is replaced by the kinetic energy density. Then, the difference between short-dashed and dashed curves is due to this approximation. The short-dashed curve is obtained by taking $\kappa = 0.4$ under this approximation. The similarity between solid and short-dashed curves means that the deviation due to this approximation is canceled out by adjusting the value of κ. In the same case of Λ380 and $\kappa = 0.3$ with B1, the dotted curve is obtained by replacing the potential energy density in Eq.(2.20) to Eq.(2.21), being the approximated treatment in [45]. This approximation to use Eq.(2.21) is found to reduce masses and to increase radii.

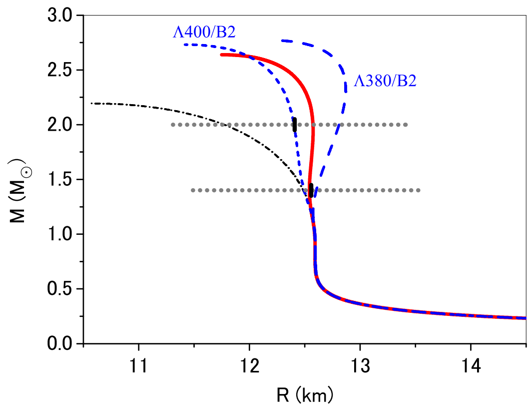

FIG. 8: (Color online) Star masses as a function of radius R. The dot-dashed curves are by the β-stable nucleonic matter EoS. The solid curve is for Λ380 with B1. Dashed and short-dashed curves are by the quarkyonic-matter EoSs for Λ380 and Λ400 with B2, respectively. The horizontal dotted lines indicates $R_{1.4M_\odot} = 12.56^{+1.00}_{-1.07}$ km and $R_{2.0M_\odot} = 12.41^{+1.00}_{-1.10}$ km.

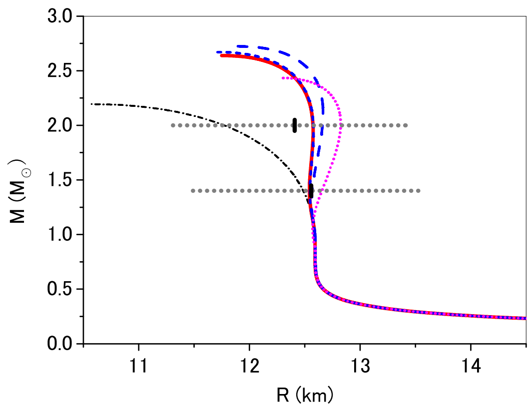

FIG. 9: (Color online) Star masses as a function of radius R. The dot-dashed curves are by the β-stable nucleonic matter EoS. The solid curve is obtained by the quarkyonic-matter EoS for Λ380 with $\kappa = 0.3$ in the case of using B1. The dashed (short-dashed) curve is for Λ380 with $\kappa = 0.3$ ($\kappa = 0.4$) by the approximation to neglect potential sectors in quark energy densities. The dotted curve is obtained by replacing the potential energy density in Eq.(2.20) to Eq.(2.21). The horizontal lines indicates $R_{1.4M_\odot} = 12.56^{+1.00}_{-1.07}$ km and $R_{2.0M_\odot} = 12.41^{+1.00}_{-1.10}$ km.

C. Discussion

In [7], they present the neutron-star properties such as maximum mass, radius, tidal deformability, pressure and central density inferred from their analysis, for which the median and 90% highest-probability-density credible regions are given. From Table II of [7], we choose the quantities in the case of w/J0740+6620 Miller+ in order to compare with the correspond-

TABLE I: Maximum masses M_{max}, pressures p at ρ_0, $2\rho_0$ and $6\rho_0$), radii R and tidal deformabilities Λ at $1.4M_\odot$ and $2.0M_\odot$, central densities ρ_c at $1.4M_\odot$, $2.0M_\odot$ and M_{max}. Results for the β-stable nucleonic matter EoS denoted as NUC, the QHT-matter EoS Q4 and the quarkyonic matter EoS V380 are compared with the values taken from [7].

	NUC	Q4	Λ380	Ref.[7]
$M_{max}/M_\odot$	2.19	2.40	2.64	$2.21^{+0.31}_{-0.21}$
$p(\rho_0)$ $(10^{33}\mathrm{dyn/cm}^2)$	5.27	5.27	5.27	$4.30^{+3.37}_{-3.80}$
$p(2\rho_0)$ $(10^{34}\mathrm{dyn/cm}^2)$	2.76	5.09	4.42	$4.38^{+2.46}_{-2.96}$
$p(6\rho_0)$ $(10^{35}\mathrm{dyn/cm}^2)$	6.94	12.0	22.6	$7.41^{+5.87}_{-4.18}$
$R_{1.4M_\odot}$ (km)	12.5	12.7	12.5	$12.56^{+1.00}_{-1.07}$
$R_{2.0M_\odot}$ (km)	11.8	12.5	12.6	$12.41^{+1.00}_{-1.10}$
$R_{2.0M_\odot} - R_{1.4M_\odot}$ (km)	−0.72	−0.14	+0.03	$-0.12^{+0.83}_{-0.85}$
$\Lambda_{1.4}$	779	525	473	507^{+234}_{-242}
$\Lambda_{2.0}$	128	46	49	44^{+34}_{-30}
$\rho_c(1.4M_\odot)$ $(10^{14}\mathrm{g/cm}^3)$	7.9	6.6	6.8	$6.7^{+1.7}_{-1.3}$
$\rho_c(2.0M_\odot)$ $(10^{14}\mathrm{g/cm}^3)$	12.	9.1	8.0	$9.7^{+3.6}_{-3.1}$
$\rho_c(M_{max})$ $(10^{15}\mathrm{g/cm}^3)$	1.8	1.6	1.3	$1.5^{+0.3}_{-0.4}$

ing values obtained from our QHT-matter and the quarkyonic matter EoSs. In Table I, tabulated are maximum masses M_{max}, pressures p at ρ_0, $2\rho_0$ and $6\rho_0$, radii R and dimensionless tidal deformabilities Λ at $1.4M_\odot$ and $2.0M_\odot$, central densities ρ_c at $1.4M_\odot$, $2.0M_\odot$ and M_{max}. Here, our results are for the β-stable nucleonic matter EoS denoted as NUC, the QHT-matter EoS Q4 and the quarkyonic matter EoS V380. These EoSs are adjusted so as to reproduce $R_{1.4M_\odot}$ with an accuracy of a few hundred meters. Then, the key feature of $R_{2M_\odot} \approx R_{1.4M_\odot}$ is found in the cases of Q4 and V380 EoSs, contrastively to the case of the nucleonic EoS giving $R_{2M_\odot} < R_{1.4M_\odot}$. The values of $R_{2.0M_\odot}$, central densities and tidal deformabilities for Q4 and V380 EoSs are far closer to the median values than those for nucleonic EoS, demonstrating the clear impacts of quark phases in Q4 and V380 EoSs. The deviations from the median values in the latter are considerably larger than those in the formers. Especially, the values of $\Lambda_{1.4}$ and $\Lambda_{2.0}$ for the nucleonic EoS are noted to be out of 90% credible regions.

In the case of the quarkyonic matter EoS for V380, the values of M_{max} and $p(6\rho_0)$ are found to be far larger than that for the nucleonic EoS. It is interesting that such a large value of M_{max} can be obtained straightforwardly from the quarkyonic-matter EoS, considering the implication of the large mass $(2.35 \pm 0.17)M_\odot$ for PSR J0952-0607 [4]. The reason why a large value of M_{max} is obtained n the case of the quarkyonic matter EoS is because the pressure rises rapidly in the region of $\rho_B \sim 2\rho_0$ as found in Fig.2. In the McLerran-Reddy model of the quarkyonic matter, the resulting EoS is mainly controlled by the one parameter Δ_{qyc} for Fermi-layer thickness. Then, it is difficult to reproduce simultaneously $M_{max} = 2.2M_\odot$ and $R_{2.0M_\odot} = 12.4$ km.

IV. CONCLUSION

The observed masses and radii of neutron stars give constraints on the dense matter EoSs and resulting *MR* diagrams. In this sense, the observations of massive stars over $2M_\odot$ and the NICER implication of $R_{2M_\odot} \approx R_{1.4M_\odot}$ are critically important for restricting neutron-star matter EoSs. In the case of hadronic matter, even if the nucleonic matter EoS is constructed so as to be stiff enough to give the maximum mass over $2M_\odot$, the hyperon mixing brings about a remarkable softening of the EoS. The EoS-softening by hyperon mixing can be reduced, for instance, by introducing many-body repulsions which work universally for every kind of baryons. However, such a repulsive effect does not cancel out completely the EoS softening by hyperon mixing: In the case of hadronic matter EoS with hyperon mixing, it is difficult to obtain maximum masses over $2M_\odot$. The most promising approach to solve this "hyperon puzzle" is to assume the existence of quark phases in inner cores of neutron stars, namely hybrid stars having quark matter in their cores.

When quark deconfinement phase transitions from a hadronic-matter EoS to a sufficiently stiff quark-matter EoS are taken into account in the neutron-star interiors, repulsive effects such as QQ repulsions in quark phases are needed in order to obtain sufficiently stiff EoSs resulting in massive hybrid stars with masses over $2M_\odot$. In our QHT matter, it is possible to reproduce maximum masses over $2M_\odot$ consistently with the NICER implication, where the QQ repulsion is taken to be strong enough and the quark-hadron transition density is adjusted so as to be about $2\rho_0$ by tuning of the density dependence of effective quark mass.

In the quarkyonic matter, the degrees of freedom inside the Fermi sea are treated as quarks, and nucleons exist at the surface of the Fermi sea. The existence of free quarks inside the Fermi sea gives nucleons extra kinetic energy by pushing them to higher momenta. This mechanism of increasing pressure is completely different from the above mechanism of EoS stiffening by strong QQ repulsions in the QHT matter. In calculations of *MR* diagrams with the quarkyonic-matter EoS, the critical quantity is the thickness Δ_{qyc} of Fermi layer controlled by the parameters Λ and κ. With the reasonable choice of these parameters, the *MR* curves of quarkyonic hybrid stars are obtained so as to be consistent with the NICER implication.

As well as $R_{2.0M_\odot}$, central densities and tidal deformabilities are inferred from the analysis of the NICER data. The QHT-matter and quarkyonic EoSs can be adjusted so as to reproduce these inferred quantities far closer to the median values than those for nucleonic matter EoS, demonstrating the clear impacts of quark phases in these cases..

Thus, the reasonable *MR* curves of neutron stars can be derived from both QHT-matter and quarkyonic-matter EoSs, having completely different mechanisms to stiffen EoSs. However, when both EoSs are adjusted so as to be consistent with the NICER implication, the maximum mass for the quakyonic-matter EoS is considerably larger than that for the QHT-matter EoS.

Acknowledgments

The authors would like to thank D. Blaschke for valuable comments and fruitful discus-

sions.

---

[1] P.B. Demorest, T. Pennucci, S.M. Ransom, M.S.E. Roberts, and J.W. Hessels, Nature (London) **467**, 1081 (2010).

[2] J. Antoniadis *et al.*, Science **340**, 6131 (2013).

[3] H.T. Cromartie *et al.*, Nat. Astron. **4**, 72 (2020).

[4] R.W. Romani *et al.*, Astrophysical J. Lett. 934:L17 (2022).

[5] M.C. Miller, et al.. Astrophys. J. Lett. **918**, L28 (2021), arXiv:2105.06979 [astro-ph.HE]

[6] T.E. Riley, et al.. Astrophys. J. Lett. **918**, L27 (2021), arXiv:2105.06980 [astro-ph.HE]

[7] I. Legred, K. Chatziioannou, R. Essick, S. Han, and P. Landy, Phys. Rev. D **104**. 063003 (2021),

[8] I. Bednarek, P. Haensel, J.L. Zdunik, M. Bejger, and R. Mańka, Astronomy & Astrophysics A**157**, 543 (2012).

[9] S. Weissenborn, D. Chatterjee, and J. Schaffner-Bielich, Nucl. Phys. A**881**, 62 (2012).

[10] M. Oertel, C.Providência, F. Gulminelli, and Ad.R. Raduta, J. Phys. G.**42** 075202 (2015).

[11] K.A. Maslov, E.E. Kolomeitsev, and D.N. Voskresensky, Phys. Lett. B**748** 369 (2015).

[12] S. Nishizaki, Y. Yamamoto, and T. Takatsuka, Prog. Theor. Phys. **105**, 607 (2001); **108**, 703 (2002).

[13] I. Vidaña,D. Logoteta, C. Providência, A. Polls, and I. Bombaci, Eur.Phys.Lett. **94**, 1002 (2011).

[14] Y. Yamamoto, T. Furumoto. Yasutake, and Th.A Rijken, Phys Rev. C bf 90 045805 (2014).

[15] Y. Yamamoto, T. Furumoto, N. Yasutake, and Th.A Rijken, Eur. Phys. J. A**52**, 19 (2016).

[16] Y. Yamamoto, H. Togashi, T. Tamagawa. T. Furumoto, N. Yasutake, and Th.A. Rijken, Phys. Rev. C**96**, 065804 (2017).

[17] D. Lonardoni A. Lovato, S. Gandolfi, and F. Pederiva, Phys. Rev. Lett. **114**, 092301 (2015).

[18] D. Logoteta, I. Vidaña, I. Bombaci, Eur. Phys. J. A**55**, 207 (2019).

[19] D. Cerstung, N. Kaiser. and W. Weise, Eur. Phys. J. A**56**, 175 (2020).

[20] A. Drago, A. Lavagno, G. Pagliara, and D. Pigato, Phys. Rev. C**90**, 065809 (2014).

[21] D.B. Kaplan, A.E. Nelson, Phys. Lett. B**175**, 57 (1986); **179**, 409 (1986).

[22] G.E. Brown, C.-H. Lee, M. Rho, and V. Thorsson, Nucl. Phys. A**567**, 937 (1994).

[23] V. Thorsson, M. Prakash, and J.M. Lattimer, Nucl. Phys. A**572**, 693 (1994).

[24] C.-H. Lee, Phys. Rep. **275**, 255 (1996).

[25] N.K. Glendenning and J. Schaffner-Bielich, Phys. Rev. Lett. **81**, 4564 (1998).

[26] M.Baldo, G.F. Burgio, and H-J. Schulze, *Superdense QCD Matter and Compact stars (NATO Science Series 2: Mathematics, Physics and Chemistry vol.197)* (2006) ed D.Blaschke and D. Sedrakian.

[27] F. Özel, D. Psaltis, S. Ransom, P. Demorest, and M. Alford, Astrophys. J. Lett. **724**, L199 (2010).

[28] I. Sagert, G. Pagliara, M, Hempel, and Schaffner-Bielich, Astrophys. J. Lett. **740**, L14 (2011).

[29] T. Kähn, D. Blaschke, and D. Lastowiecki, Phys. Rev. D**88**, 085001 (2013).

[30] L. Bonanno and A. Sedrakian, Astrophys. J**539**, 416 (2012).

[31] R. Lastowiecki, D. Blaschke, H. Grigorian, and S. Typel, Acta Phys. Pol. **B5**, 535 (2012).

[32] M. Shahrbaf, D. Blaschke, A.G. Grunfeld, and H.R. Moshfegh, Phys. Rev. **C101**, 025807 (2020).

[33] M. Shahrbaf, D. Blaschke, and S. Khanmohamadi, J. Phys. G: Nucl. Part. Phys. **47**, 115201 (2020).

[34] K. Otto, M. Oertel, and B-J Schaefer, Phys. Rev. **D101**, 103021 (2020); arXiv:1910.11929 (2020)

[35] T. Kojo, G. Baym, and T. Hatsuda, Astrophys. J. **934**, 46 (2022), arXiv:2111.11919 (2022).

[36] Y. Yamamoto, N. Yasutake, and Th. A. Rijken, Phys. Rev. **C105**, 015804 (2022).

[37] A. Akmal, V.R. Pandharipande, and D.G. Ravenhall, Phys. Rev. C**58**, 1804 (1998).

[38] A.B. Kaidalov and K.A. Ter-Materosian, Nucl. Phys. **B75**, 471 (1974).

[39] M. M. Nagels, Th. A. Rijken, and Y. Yamamoto, Phys. Rev. **C99**, 044002 (2019).
[40] M. M. Nagels, Th. A. Rijken, and Y. Yamamoto, Phys. Rev. **C99**, 044003 (2019).
[41] M. M. Nagels, Th. A. Rijken, and Y. Yamamoto, Phys. Rev. **C102**, 054003 (2020).
[42] H. Togashi and M. Takano, Nucl. Phys. A**902**, 53 (2013).
[43] L. McLerran and H.D. Pisarski, Nucl. Phys. A**796**, 83 (2007).
[44] Y. Hidaka, L. McLerran, and H.D. Pisarski, Nucl. Phys. A**808**, 117 (2008).
[45] L. McLerra and S. Reddy, Phys. Rev. Lett. **122**, 122701 (2019).
[46] S. Han, M.A.A. Mamun, S. Lalit, C. Constantinou, and M. Prakash, Phys. Rev. D**100**, 103022 (2019).
[47] D.C. Duarte, S. Hernande-Ortiz, and K.S. Jeong, Phps. Rev. C**102**, 025203 (2020); 065202 (2020).
[48] T. Zhao and J.M. Lattimer, Phys. Rev. **D102**, 023021 (2020).
[49] J. Margueron, H. Hansen, and P. Proust, and G.Chanfray, Phys. Rev. **C104**, 055803 (2021).
[50] G. Cao Phys. Rev. **D105**, 114020 (2022).
[51] N.K. Glendenning, Phys. Rev. **D46**, 1274 (1992).
[52] G. Baym, A. Bethe, and C. Pethick, Nucl. Phys. A**175**, 225 (1971).
[53] G. Baym, C.J. Pethick, and P. Sutherland, Astrophys. J.**170**, 299 (1971).